Check for updates

Geophysical Research Letters

RESEARCH LETTER
10.1029/2023GL102833

Diverging Northern Hemisphere Trends in Meteorological Versus Ecological Indicators of Spring Onset in CMIP6

Xiaolu Li[1], Toby Ault[1], Colin P. Evans[1], Flavio Lehner[1,2], Carlos M. Carrillo[1], Alison Donnelly[3], Theresa Crimmins[4], Amanda S. Gallinat[3], and Mark D. Schwartz[3]

[1]Department of Earth and Atmospheric Sciences, Cornell University, Ithaca, NY, USA, [2]Climate and Global Dynamics Laboratory, National Center for Atmospheric Research, Boulder, CO, USA, [3]Department of Geography, University of Wisconsin-Milwaukee, Milwaukee, WI, USA, [4]USA National Phenology Network, School of Natural Resources and the Environment, University of Arizona, Tucson, AZ, USA

Abstract Plant phenology regulates the carbon cycle and land-atmosphere coupling. Currently, climate models often disagree with observations on the seasonal cycle of vegetation growth, partially due to how spring onset is measured and simulated. Here we use both thermal and leaf area index (LAI) based indicators to characterize spring onset in CMIP6 models. Although the historical timing varies considerably across models, most agree that spring has advanced in recent decades and will continue to arrive earlier with future warming. Across the Northern Hemisphere for the periods 1950–2014, 1981–2014, and 2015–2099 in the historical and SSP5-8.5 simulations, thermal-based indicators estimate spring advances of -0.7 ± 0.2, -1.4 ± 0.4, and -2.4 ± 0.7 days/decade, while LAI-based indicators estimate -0.4 ± 0.3, -0.1 ± 0.3, and -1 ± 1.1 days/decade. Thereby, LAI-based indicators exhibit weaker trends toward earlier onset, leading to uncertainties from different indices being as large or larger than model uncertainty. Reconciling these discrepancies is critical for understanding future changes in spring onset.

Plain Language Summary The timing of spring onset as indicated by green-up affects plants, bird and insect populations, rivers, and agriculture. However, state-of-the-art land surface models disagree with satellite-derived records on the seasonal cycles of vegetation growth, making it difficult to accurately predict green-up, its response to climate, and the ecological consequences. Here we calculate two sets of spring onset indicators using climate model outputs to characterize spring onset variations and trends in the recent past and future. We find spring has been advancing in recent decades and will continue to arrive earlier with future warming. Thermal-based indicators show that spring onset advances by −0.7, −1.4, and −2.4 days/decade in the Northern Hemisphere during 1950–2014, 1981–2014, and 2015–2099, respectively. This result suggests that spring onset today is on average four days earlier than spring onset 30 years ago and this rate will nearly double in the future. However, compared to meteorological-based indicators, vegetation growth-based indicators exhibit weaker trends toward earlier onset. Therefore, how we define and measure spring onset, as well as the models we use to predict changes in the environmental factors, influence future changes in the start of spring.

Key Points:

- Divergence between thermal- and growth-based spring onset indicators grows with time as global temperatures increase
- Thermal-based indicators estimate spring advances of −0.7, −1.4, and −2.4 days/decade in 1950–2014, 1981–2014, and 2015–2099
- Vegetation growth-based indicators exhibit weaker trends toward earlier spring onset and larger disagreements among models

Supporting Information:

Supporting Information may be found in the online version of this article.

Correspondence to:

X. Li,
xl552@cornell.edu

Citation:

Li, X., Ault, T., Evans, C. P., Lehner, F., Carrillo, C. M., Donnelly, A., et al. (2023). Diverging Northern Hemisphere trends in meteorological versus ecological indicators of spring onset in CMIP6. *Geophysical Research Letters*, *50*, e2023GL102833. https://doi.org/10.1029/2023GL102833

Received 10 JAN 2023
Accepted 27 FEB 2023

Author Contributions:

Conceptualization: Xiaolu Li, Toby Ault, Flavio Lehner
Data curation: Xiaolu Li
Formal analysis: Xiaolu Li
Funding acquisition: Toby Ault
Investigation: Xiaolu Li
Methodology: Xiaolu Li, Toby Ault
Project Administration: Toby Ault
Software: Toby Ault
Supervision: Toby Ault
Validation: Xiaolu Li
Writing – original draft: Xiaolu Li

© 2023 The Authors.
This is an open access article under the terms of the Creative Commons Attribution-NonCommercial License, which permits use, distribution and reproduction in any medium, provided the original work is properly cited and is not used for commercial purposes.

1. Introduction

Understanding spring plant phenology is essential as it modulates ecosystem functions, the terrestrial carbon cycle, and land-atmosphere coupling (Morisette et al., 2009; Renner & Zohner, 2018; Richardson et al., 2013). In temperate and boreal regions, plant phenology modifies the terrestrial carbon cycle by governing growing season onset and duration (Morisette et al., 2009; Richardson et al., 2009, 2010). In addition, plant phenophase changes regulate land-atmosphere energy and momentum exchanges (Richardson et al., 2013; Schwartz, 1992), and therefore influence land-atmosphere coupling strength, as demonstrated by both observations (Berg et al., 2016; Findell et al., 2015; Green et al., 2017) and model experiments (Guillevic et al., 2002; Levis & Bonan, 2004; Li, Ault, Richardson, et al., 2023; Lorenz et al., 2013; Puma et al., 2013; Xu et al., 2020). Human-induced changes in temperature and precipitation will likely modify plant phenology in the future, which in turn will affect carbon sequestration and energy exchanges between the biosphere and the atmosphere (Morisette et al., 2009; Richardson et al., 2013). Therefore, understanding and evaluating phenology variabilities at high temporal resolution is critical for accurate climate projections.

Writing – review & editing: Xiaolu Li, Toby Ault, Colin P. Evans, Flavio Lehner, Carlos M. Carrillo, Alison Donnelly, Theresa Crimmins, Amanda S. Gallinat, Mark D. Schwartz

Two approaches have been widely adopted to simulate how spring onset responds to climate variability and long-term warming. First, indicator models developed from plant phenophase change dates on the ground (e.g., bud burst, blooming), like the spring indices, have been extensively used to characterize trends and variability of spring onset and identify the influence of abiotic factors (Ault, Zurita-Milla, et al., 2015; Chuine et al., 1998; Jolly et al., 2005; Schwartz et al., 2006). Because these indicator models do not modulate meteorological variables and focus on specific growth stages (e.g., leaf out) instead of carbon allocation during vegetation growth, they can be more complex and finely tuned to specific species or plant functional types (PFT) than phenology schemes in land surface models (LSMs; Krinner et al., 2005; Milly et al., 2014; Sitch et al., 2003) and require less computing resource to calculate. In addition, as they only rely on meteorological variables and can be applied and compared uniformly across models, indicator models have been adopted to estimate projected spring onset variability (Allstadt et al., 2015; Zhu et al., 2019) and used as independent indicators of climate change influences on ecosystems (Lindsey & Newman, 1956; Root et al., 2005). However, as temperature increases, the relative importance of meteorological factors like temperature and soil moisture in regulating spring onset timing and plant sensitivity to meteorological factors may change (Flynn & Wolkovich, 2018; Fu et al., 2015; Laube et al., 2014; Park et al., 2021; Parmesan, 2007; Renner & Zohner, 2018), increasing uncertainty in how natural and managed ecosystems will adapt to climate change.

Simulating plant phenology using LSMs is another approach for predicting phenology changes in the future and their influences on the Earth system. State-of-the-art LSMs adopt environmental conditions (i.e., temperature, soil moisture, etc.) to simulate plant phenology prognostically (e.g., Krinner et al., 2005; Oleson et al., 2013), but large discrepancies are present in both the amplitude of leaf area index (LAI) and land surface phenology simulated by climate models and derived from satellite imagery (Li et al., 2022; Mahowald et al., 2016; Park & Jeong, 2021; Peano et al., 2019, 2021; Richardson et al., 2012; Song et al., 2021), potentially inducing large influences on land surface states including surface temperature (Li et al., 2023; Lorenz et al., 2013; Xu et al., 2020). In addition, although plant phenology is often simulated at daily or higher temporal resolution in LSMs (Krinner et al., 2005; Oleson et al., 2013; Sitch et al., 2003), model output is often documented at a coarser resolution in the history files and therefore most evaluations are based on monthly averages, adding to uncertainties and undermining the trends (Park & Jeong, 2021; Peano et al., 2021; Song et al., 2021). Meanwhile, not all climate models simulate plant phenology and the carbon cycle prognostically (e.g., as shown in Table S1 in Supporting Information S1, nine out of the 26 models prescribe their leaf phenology from satellite data), posing additional uncertainties in future projections of land-atmosphere interactions and terrestrial carbon cycles.

Here we adopt both a suite of thermal-based indicators—the extended spring indices models (SI-x; Ault, Schwartz, et al., 2015; Ault, Zurita-Milla, et al., 2015; Schwartz et al., 2013)—and plant phenology from the Coupled Model Intercomparison Project Phase 6 (CMIP6; Eyring et al., 2016) to characterize the timing and variation of spring onset in CMIP6 simulations. While both indicators are widely used to infer changes in seasonal transitions and plant phenology, they are yet to be compared in the instrumental period and future projections. We aim to assess the historical and projected variabilities and uncertainties of spring onset timing in the Northern Hemisphere (NH), which play an important role in modulating both the carbon cycle and land-atmosphere interactions.

2. Data and Methods

2.1. CMIP6 Models

We obtained daily maximum and minimum surface air temperature and LAI from participating models in the CMIP6 ensemble from both historical and SSP5-8.5 scenario simulations (Eyring et al., 2016; O'Neill et al., 2016; see Text S1 in Supporting Information S1 for details). To estimate changes in the timing of spring onset under the most pessimistic conditions, we adopted the SSP5-8.5 scenario (hereafter SSP585) which estimates a +8.5 W/m^2 increase in radiative forcing and represents a high-emission, high-end forcing pathway (O'Neill et al., 2016). We used 1950–2099 daily maximum and minimum surface air temperature from all 26 models with both historical and SSP585 daily temperature data available (Table S1 in Supporting Information S1). Seven models also have prognostic carbon cycle and daily LAI available (Table S2 and Text S1 in Supporting Information S1). For models with leap years, we removed temperature and LAI data for Feb 29th to form a consistent comparison among models. We used bilinear interpolation to adapt all model outputs to a 1° × 1° latitude-longitude resolution.

19448007, 2023, 8, Downloaded from https://agupubs.onlinelibrary.wiley.com/doi/10.1029/2023GL102833 by Cornell University, Wiley Online Library on [26/04/2023]. See the Terms and Conditions (https://onlinelibrary.wiley.com/terms-and-conditions) on Wiley Online Library for rules of use; OA articles are governed by the applicable Creative Commons License

19448007, 2023, 8, Downloaded from https://agupubs.onlinelibrary.wiley.com/doi/10.1029/2023GL102833 by Cornell University, Wiley Online Library on [26/04/2023]. See the Terms and Conditions (https://onlinelibrary.wiley.com/terms-and-conditions) on Wiley Online Library for rules of use; OA articles are governed by the applicable Creative Commons License

2.2. The SI-x Model

The SI-x and their predecessors, the original SI were developed from historical records of lilac and honeysuckle phenology, and have been extensively used as proxies for certain groups of species, as well as to assess the impact of abiotic changes on spring onset (Ault, Schwartz, et al., 2015; Gerst et al., 2020; Schwartz et al., 2006, 2013). SI-x uses daily temperatures and latitude to estimate the timing of spring foliage (first leaf, hereafter SI-x leaf) and blooming (first bloom) for plants with temperature-responsive phenology. Here we calculated SI-x leaf for all 26 models at $1° \times 1°$ resolution from 1950 to 2099 and the observations from 1950 to 2014 (Berkeley Earth, see Text S2 in Supporting Information S1) and 1979–2014 (CPC, Text S2 in Supporting Information S1). More details of SI-x and our process can be found in Text S3 in Supporting Information S1.

2.3. LAI Threshold-Based Day of Year (DOY)

We also calculated spring onset indicators based on the DOY LAI reaches pre-defined thresholds of its annual dynamical range. The dynamical range of LAI is defined as the difference between minimum (winter) and maximum (summer) LAI each year. We focused on the 25%, 50%, and 75% thresholds of the annual dynamical range of LAI (Figure S1 in Supporting Information S1). Using threshold-based indicators reduces the influence of land-use change as well as differences in peak LAI from one year to the next (White et al., 1997). Similar methods have been adopted to determine the start of the growing season from monthly records (e.g., Peano et al., 2021; Richardson et al., 2012; Song et al., 2021), and with daily LAI we were able to achieve more precise timing and compare it with DOY records from thermal-based indicator models. Previous work suggested that the 50% threshold or the largest derivatives are better indicators of phenological changes (e.g., White et al., 2009), and here we focused on the LAI25% indicator as it is close to both the SI-x leaf timing and the 50% threshold and because we are interested in the trends and variability of the full possible ranges of spring onset, especially the early spring events. We note, however, trends and variabilities are similar among different LAI thresholds in the same model. To evaluate simulated LAIs and investigate how the phenology schemes influence model performance, we also adopted satellite imagery derived LAIs from the Global LAnd Surface Satellite project (GLASS; Liang et al., 2013, 2020) and land cover type data from Moderate Resolution Imaging Spectroradiometer (MODIS; MCD12Q1; Friedl et al., 2010; Figure S2a and Text S2 in Supporting Information S1).

2.4. Statistical Method

We calculated linear trends of the indices over different time windows and used a one-sided 5% significance level to evaluate the significance of all analyzed trends. When calculating correlations between the indicators, we first removed the linear trend and then calculated correlation coefficients of the detrended time series (Text S4 in Supporting Information S1). The significance of the trends and correlations have been adjusted for false discovery by recalculating the significance level to control the expectation of falsely rejected hypotheses (Benjamini & Hochberg, 1995).

3. Results

3.1. Spring Onset Timing

Spring onset timing has advanced in recent decades in both observations and model simulations and will shift earlier under the SSP585 scenario (Figure 1). Over 1950–2014 in the NH, CMIP6 ensemble mean of 26 models indicates 117.0 ± 6.0 days to first leaf based on the SI-x models (hereafter CMIP6-leaf), later than SI-x leaf calculated from Berkeley Earth (hereafter Obs-Berkeley-leaf, 107.3 ± 2.2 days; Figure S3a in Supporting Information S1). Over the historical period, the spread of spring onset timing in CMIP6 encompasses the interannual variability of observation-based SI-x (Figure 1a). Under the SSP585 scenario in 2015–2099, CMIP6-leaf advances to 104.5 ± 8.6 days. The largest disagreement of mean onset dates between CMIP6 models is present in Western NA, Northern Russia, and over the Tibetan Plateau during the historical period, and this spatial pattern persists into the SSP585 period (Figures S4h and S4j in Supporting Information S1).

Models experience considerable differences in simulated plant phenology (Figures S1, S3c, and S3d in Supporting Information S1), mean LAI values (Figure S5 in Supporting Information S1), and mean LAI threshold-based spring onset timing (Figures S1, S3c, S3d, and S6a in Supporting Information S1). Compared to GLASS LAI, ensemble mean overestimates LAI values in Eastern Asia and western Canada and underestimates LAI in

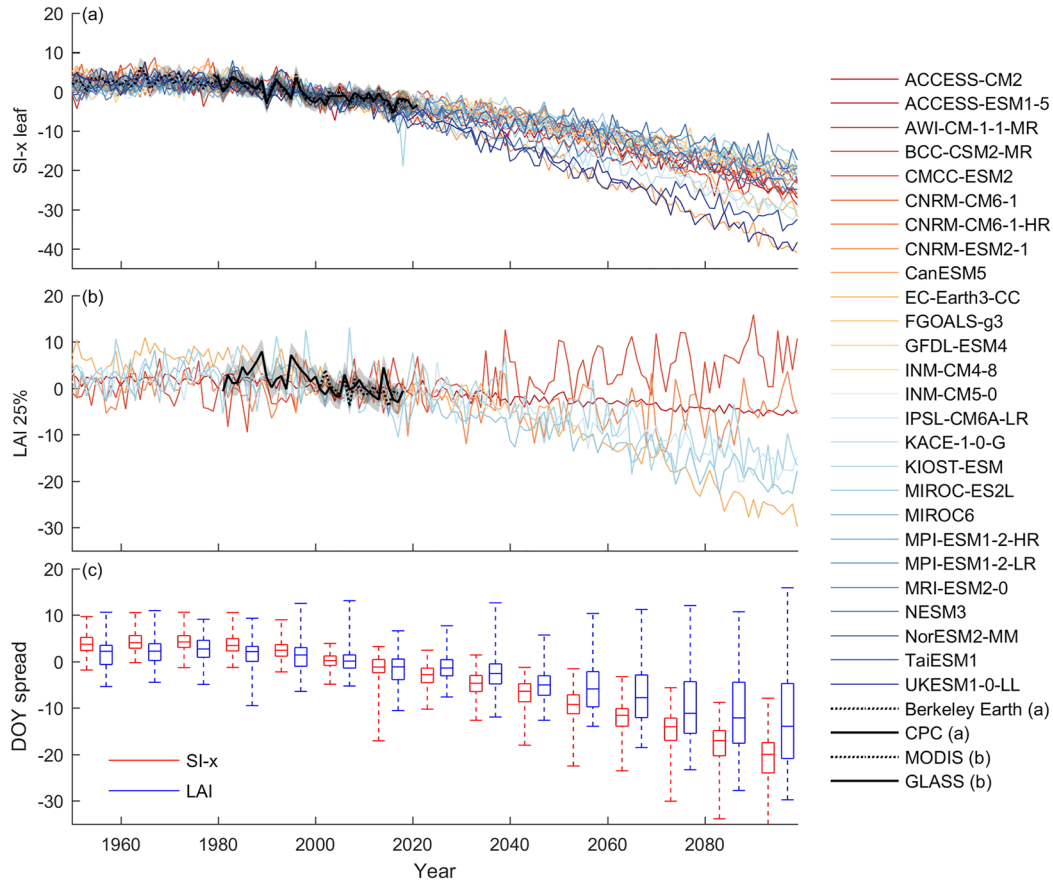

Figure 1. Anomalies in the day of year (DOY) spring onset is predicted. (a) Anomalies of the extended spring indices (SI-x) first leaf DOYs calculated from the 26 CMIP6 models and the Berkeley Earth (dotted black line) and CPC (solid black line) gridded daily temperature datasets averaged across the Northern Hemisphere (NH) (25°–85°N) and adjusted for area weight. Day-of-year (DOY) anomalies are calculated by subtracting the 1981–2010 mean of each model/observation. Each observational data set's one standard deviation interval is shown in a gray shade around its mean in panels (a) and (b). (b) Anomalies of the leaf area index (LAI) 25% threshold DOYs calculated from the seven CMIP6 models and GLASS (solid black line) and MODIS (dotted black line) LAI averaged across the NH (25°–85°N). DOY anomalies are calculated by subtracting the 2001–2014 mean of each model/observation and adjusting for area weight. (c) Box plots showing the spread of SI-x leaf and LAI25% DOYs derived from CMIP6 models during each decade. For each box plot, the centerline denotes the median of the DOYs, box limits show the upper and lower quartiles (25% and 75%), and whiskers indicate the 5% and 95% values.

Southern Russia (Figure S5 in Supporting Information S1). Large disagreements exist among the models in Canada, Northern Europe, and East Asia. These regions continue experiencing large differences among model LAIs in SSP585, along with Eastern US.

The start of spring as indicated by LAI 25% threshold DOYs also advances in the SSP585 scenario but is much later in the models than in GLASS LAI in the historical period (Figure S3c in Supporting Information S1). Across the NH, mean LAI 25% DOY based on simulated LAIs (hereafter CMIP6-LAI25%) is 137.7 ± 19.7 during 1981–2014, 20 days later than in GLASS LAI (hereafter Obs-GLASS-LAI25%, 117.9 ± 2.6). CMIP6-LAI25% advances to 134.9 ± 24.4 in 2015–2099 in SSP585. The timing varies considerably across models (Figure 1b, Figures S3c, S3d, and S6a in Supporting Information S1). The largest disagreement among models is present south of 40°N while large differences between CMIP6-LAI25% and Obs-GLASS-LAI25% are also present in the Tibetan Plateau, Russia, and Northern Europe. Overall, models estimate later spring onset over high-latitude (north of 55°N) and high-elevation regions (Figure S7 in Supporting Information S1). In addition, in every period, CMIP6-LAI25% exhibits larger inter-model variability than CMIP6-leaf (Figure 1c, Figures S4g–S4j in Supporting Information S1). Differences between SI-x leaf and LAI25% vary across models and regions but overall the discrepancies between indicators increase through time.

19448007, 2023, 8, Downloaded from https://agupubs.onlinelibrary.wiley.com/doi/10.1029/2023GL102833 by Cornell University, Wiley Online Library on [26/04/2023]. See the Terms and Conditions (https://onlinelibrary.wiley.com/terms-and-conditions) on Wiley Online Library for rules of use; OA articles are governed by the applicable Creative Commons License

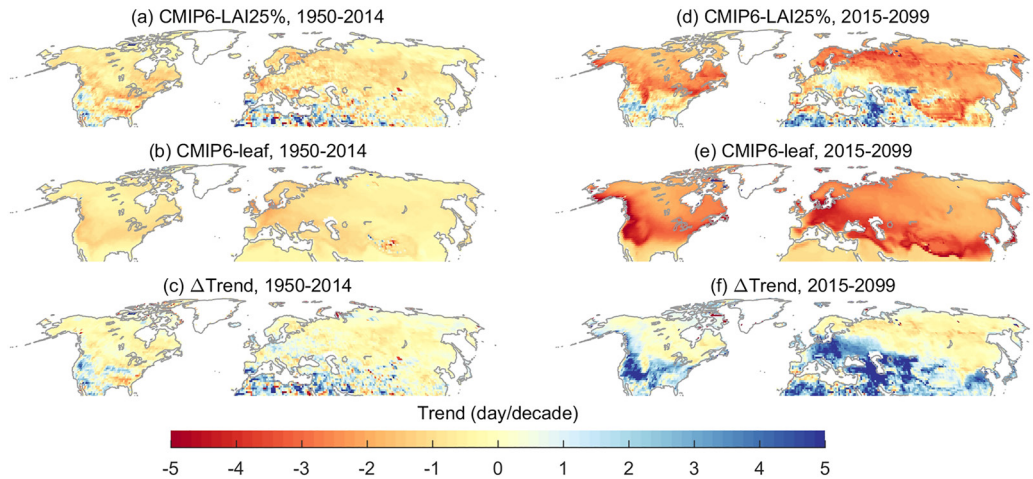

Figure 2. Ensemble mean and differences of spring onset trends. (a, b, d, e) Ensemble mean trends of leaf area index 25% threshold day of year (CMIP6-LAI25%) and extended spring indices first leaf (CMIP6-leaf) during the historical (1950–2014) and SSP585 (2015–2099) periods (unit: day/decade). (c, f) Differences in mean trends between CMIP6-LAI25% and CMIP6-leaf. CMIP6-LAI25% trends are based on seven models and CMIP6-leaf trends are averaged across 26 models.

3.2. Trends in the Start of Spring

Long-term trends in the start of spring, as measured by SI-x leaf trends over 1950–2014, exhibit overall agreement between observations and the ensemble mean but vary considerably across models (Figures S8a, S8b, and S9 in Supporting Information S1). During 1950–2014 in the NH, the ensemble mean trend of CMIP6-leaf is -0.72 ± 0.21 days/decade, whereas the mean Obs-Berkeley-leaf trend is -0.85 days/decade (Figures S8a and S8b in Supporting Information S1). The magnitude of these trends increases during the more recent period (1981–2014), with CMIP6-leaf mean trend of -1.44 ± 0.4 days/decade, slightly greater than Obs-Berkeley-leaf (-1.28 days/decade) and CPC (Obs-CPC-leaf, -1.21 days/decade). During 2015–2099, CMIP6-leaf exhibits an ensemble mean trend of -2.39 ± 0.71 days/decade. However, the trends vary considerably across models and even among different members of the same model (Figures S8a and S8b in Supporting Information S1).

The spatial pattern of spring advancement exhibits large variations among models and between the ensemble mean and observations. Both Obs-Berkeley-leaf and Obs-CPC-leaf exhibit relatively large advancement in the Tibetan Plateau, North Russia, and Southern Europe during 1981–2014 (Figure S9 in Supporting Information S1), and trends in central and north Asia are statistically significant in Obs-CPC-leaf. This pattern is not present in CMIP6-leaf or any individual model-based SI-x leaf. Moreover, models exhibit significant trends in very few regions (e.g., Eastern NA and Europe in EC-Earth-3-CC and mid-to-high latitude regions in Asia in GFDL-ESM4). The greatest earlier trend in the ensemble mean is in Southern Europe, Eastern US, and the eastern and southern parts of the Rocky Mountains (Figures 2b and 2e), but these regions also exhibit large disagreements among models (Figures S9 and S10b in Supporting Information S1). When compared to observations, CMIP6-leaf tends to overestimate spring advancement in NA, particularly Western Canada and Eastern US, and underestimate spring advancement in central and north Asia (Figure S11 in Supporting Information S1). During 2015–2099, most models exhibit significant earlier spring across the NH (Figures S12b and S13f in Supporting Information S1) and the greatest earlier trend is present in regions along the Pacific coast of NA, in central NA, Europe, and mid-latitude regions of Asia (Figure 2e). Though models mostly agree that spring is starting earlier under the historical and future scenarios (Figures S10b, S12b, S13b, S13d, and S13f in Supporting Information S1), large disagreements among models are also present, with ACCESS-CM2, CMCC-ESM2, CNRM-CM6-1, CNRM-CM6-1-HR, EC-Earth3-CC, IPSL-CM6A-LR, TaiESM1, and UKESM1-0-LL experiencing a much larger earlier trend while FGOALS-g3, KIOST-ESM, MRI-ESM2-0, and NESM3 exhibiting a much smaller trend (Figures S9 and S11 in Supporting Information S1). Compared to the historical period, the magnitude of the trends and variability of CMIP6-leaf increases in 2015–2099 (Figures 1a and 1c).

Trends of CMIP6-LAI25% vary considerably geographically and across models, but also display an overall earlier spring onset and increasing variability over the NH (Figures 1b, 1c, 2a and 2d, Figures S8c, S8d, S10a, S12a, S13a, S13c, and S13e in Supporting Information S1). During 1950–2014, the mean NH trends

19448007, 2023, 8, Downloaded from https://agupubs.onlinelibrary.wiley.com/doi/10.1029/2023GL102833 by Cornell University, Wiley Online Library on [26/04/2023]. See the Terms and Conditions (https://onlinelibrary.wiley.com/terms-and-conditions) on Wiley Online Library for rules of use; OA articles are governed by the applicable Creative Commons License

19448007, 2023, 8, Downloaded from https://agupubs.onlinelibrary.wiley.com/doi/10.1029/2023GL102833 by Cornell University, Wiley Online Library on [26/04/2023]. See the Terms and Conditions (https://onlinelibrary.wiley.com/terms-and-conditions) on Wiley Online Library for rules of use; OA articles are governed by the applicable Creative Commons License

of CMIP6-LAI25% is −0.41 ± 0.31 day/decade, ∼0.3 day/decade smaller than those indicated by CMIP6-leaf (Figure S8 in Supporting Information S1). The largest trends are present along 60°N in Eurasia and Eastern NA, though trends vary across models in Southern Europe and south of 40°N. During 1981–2014, trends of both CMIP6-LAI25% (−0.05 ± 0.29) and Obs-GLASS-LAI25% (−0.01) are close to 0, likely due to the delayed start of spring in areas south of 40°N and Southern Europe (Figures S10a and S12a in Supporting Information S1), where soil moisture is the governing factors for plant growth (Figure S2 in Supporting Information S1). Though CMIP6-LAI25% mean trends are negative (i.e., spring arrives earlier) in the US, northern Canada, and southern Russia and positive in southern Europe, Obs-GLASS-LAI25% trends in these regions are of smaller amplitude, and sometimes in the opposite direction (Figure S10a in Supporting Information S1). The trends change to −0.97 ± 1.06 days/decade during 2015–2099 under the SSP585 scenario, ∼1.4 days/decade fewer than trends estimated from CMIP6-leaf. Over the 2015–2099 period, the trend is much stronger in mid-to-high latitude (north of 45°N) and high-elevation regions (Figure 2d, Figures S12a and S13e in Supporting Information S1). In southern Europe and the US, the models diverge in LAI25% responses with large positive trends (delay in spring onset) in CMCC-ESM2, negative trends in EC-Earth3-CC, IPSL-CM6A-LR, and MIROC-ES2L, and contrasting trends in CNRM-ESM2-1.

Although the timing indicated by LAI25% and SI-x leaf vary across models, variabilities and trends derived from the two sets of indicators exhibit relatively good agreement, especially during longer temporal periods and in temperature-dominant PFTs (Figures 2c, 2f and Figures S6c, S10c, S10d, S12c, and S12d in Supporting Information S1). During 1981–2014, Obs-GLASS-LAI25% exhibits weaker trends in spring onset timing than Obs-Berkeley-leaf at higher latitudes (north of 50°N) and stronger trends at low latitudes (south of 30°N). This latitudinal pattern is also present in most of the models (except KIOST-ESM) with some variations (Figure S10c in Supporting Information S1). Similar agreement of spring onset trends at mid-to-high latitudes are also present in the ensemble means based on all available models (Figure 2, Figure S14 in Supporting Information S1). Although trends of CMIP6-leaf increase faster than CMIP6-LAI25%, their variabilities are coherent and the difference in their trends is still relatively small and spatially uniform at mid-to-high latitudes. Across the NH, the spread among different indicators is smaller at higher latitudes with the smallest spread present between 55.5° and 84.5°N. However, differences between LAI- and thermal-based indicators increase in the SSP585 scenario across different latitudes, and CMIP6-LAI25% can even be delayed at lower latitudes (Figure S12 in Supporting Information S1). At mid-to-high latitudes (north of 40°N except southern Europe), both observations and models exhibit positive and significant correlations between SI-x leaf and LAI25%, except for ACCESS-ESM1-5 in the future scenario and CMCC-ESM2 and KIOST-ESM in some moisture-limited regions (Figures S2, S10d, and S12d in Supporting Information S1). Overall, models exhibit an NH mean correlation of 0.47 ± 0.22 during the historical period and 0.43 ± 0.23 under SSP585 between the two sets of indicators.

4. Discussion and Conclusion

Our results show good agreement between SI-x leaf calculated from simulated and observed temperatures, but considerable differences are present between model-simulated and observed LAI25% and between LAI25% and SI-x leaf estimated from models. Our results also confirm the later start of the growing season in models presented by previous studies (Li et al., 2022; Park & Jeong, 2021; Peano et al., 2019, 2021; Song et al., 2021). Part of the differences can be due to the uncertainties in both the gridded temperature datasets and the remote sensing derived LAI estimates we adopted here. For instance, satellite-based LAIs are derived from assumptions about land cover type and observed reflectance and therefore may be influenced by scale effects when aggregated to the relatively coarse spatial resolution of climate models (e.g., Liu et al., 2019; Zhang et al., 2017) and winter snow cover (e.g., Myneni et al., 2015). However, uncertainties in the observational datasets are relatively small compared to the inter-model as well as the between-index uncertainties (Figure 1). Although part of the between-index differences may be due to PFTs at lower latitudes where spring onset and vegetation growth are limited by both soil moisture and temperature (Table S2 and stress deciduous PFTs in Figure S2b in Supporting Information S1), our results show LAI25% exhibits a less negative trend (i.e., a less early start of spring) than SI-x leaf at all latitudes, though the indicators are positively correlated (Figure S14 in Supporting Information S1). Leaf development in LSMs depends both on spring onset timing and carbon allocation to leaves and experiences impacts of both temperature and soil moisture, so LAI threshold-based indicators reflect the combined influences of biotic and abiotic factors, while SI-x mostly follows environmental impacts. Therefore, SI-x leaf shows the full potential range of temperature-induced spring onset variability while LAI25% is more restrained by

19448007, 2023, 8, Downloaded from https://agupubs.onlinelibrary.wiley.com/doi/10.1029/2023GL102833 by Cornell University, Wiley Online Library on [26/04/2023]. See the Terms and Conditions (https://onlinelibrary.wiley.com/terms-and-conditions) on Wiley Online Library for rules of use; OA articles are governed by the applicable Creative Commons License

environmental and biotic factors and may therefore be less sensitive to temperature changes. However, the large differences in spring onset timing and trends imply that plant phenology may experience index-related variability and uncertainty as large as or larger than model uncertainty for a given index.

The timing of spring onset has been advancing over the NH, and the pace is likely to accelerate in the future. Although the start of spring trends in the most recent decade exhibit large uncertainty (Wang et al., 2019), both observations and satellite remote sensing records suggest a long-term advancing trend of spring onset timing (Ault, Schwartz, et al., 2015; Cook et al., 2012; Parmesan & Yohe, 2003; Root et al., 2003; White et al., 2009). We have similarly found earlier spring onset during 1950–2014 in both thermal- and LAI-based indicators which have also been accelerating at mid-to-high latitudes. While thermal-based indices like SI-x have been shown to be good indicators of spring onset variability (e.g., Ault, Schwartz, et al., 2015; Gerst et al., 2020) and widely adopted to assess future changes in spring onset timing (Allstadt et al., 2015; Zhu et al., 2019), other environmental factors (e.g., chilling, soil moisture, photoperiod) also influence the start of spring (Flynn & Wolkovich, 2018; Fu et al., 2015; Laube et al., 2014). In addition, changing environments may favor some species and trigger further changes in ecosystem structure and composition (Renner & Zohner, 2018; Wang et al., 2016). Studies also suggested potential regime shifts to more soil moisture-limited plant growth and land-atmosphere coupling in previously temperature-dominated regions (e.g., Denissen et al., 2022; Green et al., 2017) and thermal-based indicators may need to be adopted with more caution in these regions. Meanwhile, frost risk may also vary as climatic conditions change (Park et al., 2021; Rigby & Porporato, 2008; Zohner et al., 2020), posing additional uncertainty to how natural and managed ecosystems adapt to climate change. Therefore, it is critical to evaluate trends and variability of spring onset in climate models using both meteorological- and ecological-based indicators and update our predictions as we improve our forecasting approaches.

Agreement between thermal- and LAI-based indicators depends on the phenology schemes adopted in the climate models (Figures S10, S12, and Table S2 in Supporting Information S1), and the disagreements may further increase the uncertainty in temperature and spring onset projections. LAI- and thermal-based indicators show stronger agreement when phenology is prognostically simulated at higher temporal resolution (i.e., daily or finer). Though temperature dominates spring onset timing of LAI25% at higher latitudes, phenology schemes with only temperature criteria have a higher correlation with SI-x leaf at lower latitudes than phenology schemes with both temperature and soil moisture switches or implicit phenology. As soil moisture and precipitation can be important in triggering spring onset in moisture-limited environments (Dahlin et al., 2015, 2017), the relative importance of temperature may be overestimated in temperature-dominated phenology schemes, though trends of LAI25% still indicate less advancement in spring onset than SI-x leaf in these models. Moreover, interactions between phenology and other model components can affect the phenological triggers and further cause discrepancies in plant phenology (e.g., Li et al., 2022). As changes in phenology and growing season length modulate surface temperature (Li, Ault, Richardson, et al., 2023; Lorenz et al., 2013; Xu et al., 2020), these disagreements between thermal- and vegetation-based indicators may undermine the credibility of temperature projections and further increase the uncertainty in spring onset timing.

Leaf phenology in land surface models is determined by the phenology scheme as well as environmental factors like temperature and soil moisture, and their relative importance varies with different model settings. In models where phenology is prescribed or explicitly simulated, when growing season starts is regulated by the phenology scheme for deciduous PFTs, but leaf development also depends on carbon allocation to the leaf carbon pool and therefore photosynthesis and net primary production. For models with implicit phenology, because photosynthesis and respiration are sensitive to meteorological conditions and LAI follows biomass, LAI-based spring onset can exhibit better agreement with SI-x than models with explicit phenology schemes. In addition, models exhibit smaller discrepancies in their SI-x estimates than LAI-based indicators as variability in SI-x are mostly driven by thermal changes and the representation of air temperature is more similar in models than plant phenology. Overall, better agreement among models and between indicators are present in temperature-limited regions and divergence among models in SI-x is much smaller than that in LAI-based indicators. The largest disagreement between thermal- and vegetation-based indicators is present in more soil moisture-limited regions at mid-to-low latitudes that are mostly dominated by grasses, broadleaf forests, and crops.

Plant phenology regulates the terrestrial carbon cycle and land-atmosphere coupling in Earth system models as it influences critical processes such as photosynthesis, respiration, and evapotranspiration, yet our results show large disagreements in both the timing and trends of spring onset among models and between models and

observations. As LAI-based indicators exhibit weaker trends toward earlier onset and larger inter-model discrepancies than thermal-based indicators, the bias between LAI- and thermal-based spring onset timing may continue to increase in the future, resulting in greater uncertainties in projected spring onset timing. In certain cases, this index-based uncertainty can be larger than inter-model uncertainty for a given index. Indicator models can provide inference on spring onset trends and variability and help isolate the influence of climate factors, but larger uncertainties are present under a warmer climate due to phenology responses to other abiotic and biotic factors. Therefore, studies interested in projected changes in spring phenology should consider variabilities in both meteorological- and vegetation-based indicators, and future work should focus on understanding LAI variability and improving phenology representation in climate models.

Conflict of Interest

The authors declare no conflicts of interest relevant to this study.

Data Availability Statement

The CMIP6 model outputs (maximum and minimum daily temperature, tasmax and tasmin, and leaf area index, lai) are publicly available through the Earth System Grid Federation (ESGF): https://esgf-node.llnl.gov/projects/cmip6/. The extended spring indices first leaf and LAI25% DOYs used for this analysis are available in the Figshare repository: https://doi.org/10.6084/m9.figshare.21094264 (Li, Ault, Carrillo, et al., 2023). The code used to calculate the extended spring indices is described in detail in Ault, Zurita-Milla, et al. (2015) and is available at https://github.com/cornell-eas/SI-X.

Acknowledgments
This work is supported by NSF Macrosystems Biology award (DEB-2017815; DEB-1702551; DEB-2017831; DEB-2017848) and NSF Career Award (AGS-1751535). We thank the reviewers for their careful review and constructive comments, which greatly helped in improving this manuscript. The authors also acknowledge high-performance computing support from Cheyenne (https://doi.org/10.5065/D6RX99HX) provided by NCAR's Computational and Information Systems Laboratory.

References

Allstadt, A. J., Vavrus, S. J., Heglund, P. J., Pidgeon, A. M., Thogmartin, W. E., & Radeloff, V. C. (2015). Spring plant phenology and false springs in the conterminous US during the 21st century. *Environmental Research Letters*, *10*(10), 104008. https://doi.org/10.1088/1748-9326/10/10/104008

Ault, T. R., Schwartz, M. D., Zurita-Milla, R., Weltzin, J. F., & Betancourt, J. L. (2015). Trends and natural variability of spring onset in the coterminous United States as evaluated by a new gridded dataset of spring indices. *Journal of Climate*, *28*(21), 8363–8378. https://doi.org/10.1175/jcli-d-14-00736.1

Ault, T. R., Zurita-Milla, R., & Schwartz, M. D. (2015). A Matlab© toolbox for calculating spring indices from daily meteorological data. *Computers & Geosciences*, *83*, 46–53. https://doi.org/10.1016/j.cageo.2015.06.015

Benjamini, Y., & Hochberg, Y. (1995). Controlling the false discovery rate: A practical and powerful approach to multiple testing. *Journal of the Royal Statistical Society. Series B (Methodological)*, *57*(1), 289–300. https://doi.org/10.2307/2346101

Berg, A., Findell, K., Lintner, B., Giannini, A., Seneviratne, S. I., Van Den Hurk, B., et al. (2016). Land–atmosphere feedbacks amplify aridity increase over land under global warming. *Nature Climate Change*, *6*(9), 869–874. https://doi.org/10.1038/nclimate3029

Chuine, I., Cour, P., & Rousseau, D. D. (1998). Fitting models predicting dates of flowering of temperate-zone trees using simulated annealing. *Plant, Cell & Environment*, *21*(5), 455–466. https://doi.org/10.1046/j.1365-3040.1998.00299.x

Cook, B. I., Wolkovich, E. M., Davies, T. J., Ault, T. R., Betancourt, J. L., Allen, J. M., et al. (2012). Sensitivity of spring phenology to warming across temporal and spatial climate gradients in two independent databases. *Ecosystems*, *15*(8), 1283–1294. https://doi.org/10.1007/s10021-012-9584-5

Dahlin, K. M., Del Ponte, D., Setlock, E., & Nagelkirk, R. (2017). Global patterns of drought deciduous phenology in semi-arid and savanna-type ecosystems. *Ecography*, *40*(2), 314–323. https://doi.org/10.1111/ecog.02443

Dahlin, K. M., Fisher, R. A., & Lawrence, P. J. (2015). Environmental drivers of drought deciduous phenology in the Community Land Model. *Biogeosciences*, *12*(16), 5061–5074. https://doi.org/10.5194/bg-12-5061-2015

Denissen, J., Teuling, A. J., Pitman, A. J., Koirala, S., Migliavacca, M., Li, W., et al. (2022). Widespread shift from ecosystem energy to water limitation with climate change. *Nature Climate Change*, *12*(7), 677–684. https://doi.org/10.1038/s41558-022-01403-8

Eyring, V., Bony, S., Meehl, G. A., Senior, C. A., Stevens, B., Stouffer, R. J., & Taylor, K. E. (2016). Overview of the Coupled Model Intercomparison Project Phase 6 (CMIP6) experimental design and organization. *Geoscientific Model Development*, *9*(5), 1937–1958. https://doi.org/10.5194/gmd-9-1937-2016

Findell, K. L., Gentine, P., Lintner, B. R., & Guillod, B. P. (2015). Data length requirements for observational estimates of land–atmosphere coupling strength. *Journal of Hydrometeorology*, *16*(4), 1615–1635. https://doi.org/10.1175/jhm-d-14-0131.1

Flynn, D. F. B., & Wolkovich, E. M. (2018). Temperature and photoperiod drive spring phenology across all species in a temperate forest community. *New Phytologist*, *219*(4), 1353–1362. https://doi.org/10.1111/nph.15232

Friedl, M. A., Sulla-Menashe, D., Tan, B., Schneider, A., Ramankutty, N., Sibley, A., & Huang, X. (2010). MODIS collection 5 global land cover: Algorithm refinements and characterization of new datasets. *Remote Sensing of Environment*, *114*(1), 168–182. https://doi.org/10.1016/j.rse.2009.08.016

Fu, Y. H., Zhao, H., Piao, S., Peaucelle, M., Peng, S., Zhou, G., et al. (2015). Declining global warming effects on the phenology of spring leaf unfolding. *Nature*, *526*(7571), 104–107. https://doi.org/10.1038/nature15402

Gerst, K. L., Crimmins, T. M., Posthumus, E. E., Rosemartin, A. H., & Schwartz, M. D. (2020). How well do the spring indices predict phenological activity across plant species? *International Journal of Biometeorology*, *64*(5), 889–901. https://doi.org/10.1007/s00484-020-01879-z

Green, J. K., Konings, A. G., Alemohammad, S. H., Berry, J., Entekhabi, D., Kolassa, J., et al. (2017). Regionally strong feedbacks between the atmosphere and terrestrial biosphere. *Nature Geoscience*, *10*(6), 410–414. https://doi.org/10.1038/ngeo2957

19448007, 2023, 8, Downloaded from https://agupubs.onlinelibrary.wiley.com/doi/10.1029/2023GL102833 by Cornell University, Wiley Online Library on [26/04/2023]. See the Terms and Conditions (https://onlinelibrary.wiley.com/terms-and-conditions) on Wiley Online Library for rules of use; OA articles are governed by the applicable Creative Commons License

Guillevic, P., Koster, R. D., Suarez, M. J., Bounoua, L., Collatz, G. J., Los, S. O., & Mahanama, S. P. P. (2002). Influence of the interannual variability of vegetation on the surface energy balance—A global sensitivity study. *Journal of Hydrometeorology*, *3*(6), 617–629. https://doi.org/10.1175/1525-7541(2002)003<0617:iotivo>2.0.co;2

Jolly, W. M., Nemani, R., & Running, S. W. (2005). A generalized, bioclimatic index to predict foliar phenology in response to climate. *Global Change Biology*, *11*(4), 619–632. https://doi.org/10.1111/j.1365-2486.2005.00930.x

Krinner, G., Viovy, N., de Noblet-Ducoudré, N., Ogée, J., Polcher, J., Friedlingstein, P., et al. (2005). A dynamic global vegetation model for studies of the coupled atmosphere-biosphere system. *Global Biogeochemical Cycles*, *19*, 1. https://doi.org/10.1029/2003gb002199

Laube, J., Sparks, T. H., Estrella, N., Höfler, J., Ankerst, D. P., & Menzel, A. (2014). Chilling outweighs photoperiod in preventing precocious spring development. *Global Change Biology*, *20*(1), 170–182. https://doi.org/10.1111/gcb.12360

Levis, S., & Bonan, G. B. (2004). Simulating springtime temperature patterns in the community atmosphere model coupled to the community land model using prognostic leaf area. *Journal of Climate*, *17*(23), 4531–4540. https://doi.org/10.1175/3218.1

Li, X., Ault, T., Carrillo, C. M., Evans, C., Lehner, F., Crimmins, T. M., D., et al. (2023). "Diverging northern hemisphere trends in meteorological versus ecological indicators of Spring Onset in CMIP6" [Dataset]. Figshare. https://doi.org/10.6084/M9.FIGSHARE.21094264

Li, X., Ault, T., Richardson, A. D., Carrillo, C. M., Lawrence, D. M., Lombardozzi, D., et al. (2023). Impacts of shifting phenology on boundary layer dynamics in North America in the CESM. *Agricultural and Forest Meteorology*, *330*, 109286. https://doi.org/10.1016/j.agrformet.2022.109286

Li, X., Melaas, E., Carrillo, C. M., Ault, T., Richardson, A. D., Lawrence, P., et al. (2022). A comparison of land surface phenology in the Northern Hemisphere derived from satellite remote sensing and the Community Land Model. *Journal of Hydrometeorology*, *23*(6), 859–873. https://doi.org/10.1175/jhm-d-21-0169.1

Liang, S., Cheng, C., Jia, K., Jiang, B., Liu, Q., Xiao, Z., et al. (2020). The global LAnd surface satellite (GLASS) products suite. *Bulletin of the American Meteorological Society*, *102*(2), E323–E337. https://doi.org/10.1175/BAMS-D-18-0341.1

Liang, S., Zhao, X., Yuan, W., Liu, S., Cheng, X., Xiao, Z., et al. (2013). A long-term Global LAnd Surface Satellite (GLASS) dataset for environmental studies. *International Journal of Digital Earth*, *6*(sup1), 5–33. https://doi.org/10.1080/17538947.2013.805262

Lindsey, A. A., & Newman, J. E. (1956). Use of official wather data in spring time: Temperature analysis of an Indiana phenological record. *Ecology*, *37*(4), 812–823. https://doi.org/10.2307/1933072

Liu, L., Cao, R., Shen, M., Chen, J., Wang, J., & Zhang, X. (2019). How does scale effect influence spring vegetation phenology estimated from satellite-derived vegetation indexes? *Remote Sensing*, *11*(18), 2137. https://doi.org/10.3390/rs11182137

Lorenz, R., Davin, E. L., Lawrence, D. M., Stöckli, R., & Seneviratne, S. I. (2013). How important is vegetation phenology for European climate and heat waves? *Journal of Climate*, *26*(24), 10077–10100. https://doi.org/10.1175/jcli-d-13-00040.1

Mahowald, N., Lo, F., Zheng, Y., Harrison, L., Funk, C., Lombardozzi, D., & Goodale, C. (2016). Projections of leaf area index in earth system models. *Earth System Dynamics*, *7*(1), 211–229. https://doi.org/10.5194/esd-7-211-2016

Milly, P. C. D., Malyshev, S. L., Shevliakova, E., Dunne, K. A., Findell, K. L., Gleeson, T., et al. (2014). An enhanced model of land water and energy for global hydrologic and earth-system studies. *Journal of Hydrometeorology*, *15*(5), 1739–1761. https://doi.org/10.1175/jhm-d-13-0162.1

Morisette, J. T., Richardson, A. D., Knapp, A. K., Fisher, J. I., Graham, E. A., Abatzoglou, J., et al. (2009). Tracking the rhythm of the seasons in the face of global change: Phenological research in the 21st century. *Frontiers in Ecology and the Environment*, *7*(5), 253–260. https://doi.org/10.1890/070217

Myneni, R., Knyazikhin, Y., & Park, T. (2015). MOD15A2H MODIS/terra leaf area index/FPAR 8-day L4 global 500 m SIN grid V006. In *NASA EOSDIS land processes DAAC*.

Oleson, K. W., Lawrence, D. M., Bonan, G. B., Drewniak, B., Huang, M., Charles, D., et al. (2013). CLM 4.5 NCAR technical note. July 2013. https://doi.org/10.1007/s11538-011-9690-0

O'Neill, B. C., Tebaldi, C., Van Vuuren, D. P., Eyring, V., Friedlingstein, P., Hurtt, G., et al. (2016). The scenario model intercomparison project (ScenarioMIP) for CMIP6. *Geoscientific Model Development*, *9*(9), 3461–3482. https://doi.org/10.5194/gmd-9-3461-2016

Park, H., & Jeong, S. (2021). Leaf area index in Earth system models: How the key variable of vegetation seasonality works in climate projections. *Environmental Research Letters*, *16*(3), 34027. https://doi.org/10.1088/1748-9326/abe2cf

Park, I. W., Ramirez-Parada, T., & Mazer, S. J. (2021). Advancing frost dates have reduced frost risk among most North American angiosperms since 1980. *Global Change Biology*, *27*(1), 165–176. https://doi.org/10.1111/gcb.15380

Parmesan, C. (2007). Influences of species, latitudes and methodologies on estimates of phenological response to global warming. *Global Change Biology*, *13*(9), 1860–1872. https://doi.org/10.1111/j.1365-2486.2007.01404.x

Parmesan, C., & Yohe, G. (2003). A globally coherent fingerprint of climate change impacts across natural systems. *Nature*, *421*(6918), 37–42. https://doi.org/10.1038/nature01286

Peano, D., Hemming, D., Materia, S., Delire, C., Fan, Y., Joetzjer, E., et al. (2021). Plant phenology evaluation of CRESCENDO land surface models–Part 1: Start and end of the growing season. *Biogeosciences*, *18*(7), 2405–2428. https://doi.org/10.5194/bg-18-2405-2021

Peano, D., Materia, S., Collalti, A., Alessandri, A., Anav, A., Bombelli, A., & Gualdi, S. (2019). Global variability of simulated and observed vegetation growing season. *Journal of Geophysical Research: Biogeosciences*, *124*(11), 3569–3587. https://doi.org/10.1029/2018jg004881

Puma, M. J., Koster, R. D., & Cook, B. I. (2013). Phenological versus meteorological controls on land-atmosphere water and carbon fluxes. *Journal of Geophysical Research: Biogeosciences*, *118*(1), 14–29. https://doi.org/10.1029/2012jg002088

Renner, S. S., & Zohner, C. M. (2018). Climate change and phenological mismatch in trophic interactions among plants, insects, and vertebrates. *Annual Review of Ecology, Evolution, and Systematics*, *49*(1), 165–182. https://doi.org/10.1146/annurev-ecolsys-110617-062535

Richardson, A. D., Anderson, R. S., Arain, M. A., Barr, A. G., Bohrer, G., Chen, G., et al. (2012). Terrestrial biosphere models need better representation of vegetation phenology: Results from the North American Carbon Program Site Synthesis. *Global Change Biology*, *18*(2), 566–584. https://doi.org/10.1111/j.1365-2486.2011.02562.x

Richardson, A. D., Andy Black, T., Ciais, P., Delbart, N., Friedl, M. A., Gobron, N., et al. (2010). Influence of spring and autumn phenological transitions on forest ecosystem productivity. *Philosophical Transactions of the Royal Society B: Biological Sciences*, *365*(1555), 3227–3246. https://doi.org/10.1098/rstb.2010.0102

Richardson, A. D., Hollinger, D. Y., Dail, D. B., Lee, J. T., Munger, J. W., & O'keefe, J. (2009). Influence of spring phenology on seasonal and annual carbon balance in two contrasting New England forests. *Tree Physiology*, *29*(3), 321–331. https://doi.org/10.1093/treephys/tpn040

Richardson, A. D., Keenan, T. F., Migliavacca, M., Ryu, Y., Sonnentag, O., & Toomey, M. (2013). Climate change, phenology, and phenological control of vegetation feedbacks to the climate system. *Agricultural and Forest Meteorology*, *169*, 156–173. https://doi.org/10.1016/j.agrformet.2012.09.012

Rigby, J. R., & Porporato, A. (2008). Spring frost risk in a changing climate. *Geophysical Research Letters*, *35*, 12. https://doi.org/10.1029/2008gl033955

19448007, 2023, 8, Downloaded from https://agupubs.onlinelibrary.wiley.com/doi/10.1029/2023GL102833 by Cornell University, Wiley Online Library on [26/04/2023]. See the Terms and Conditions (https://onlinelibrary.wiley.com/terms-and-conditions) on Wiley Online Library for rules of use; OA articles are governed by the applicable Creative Commons License

Root, T. L., MacMynowski, D. P., Mastrandrea, M. D., & Schneider, S. H. (2005). Human-modified temperatures induce species changes: Joint attribution. *Proceedings of the National Academy of Sciences*, *102*(21), 7465–7469. https://doi.org/10.1073/pnas.0502286102

Root, T. L., Price, J. T., Hall, K. R., Schneider, S. H., Rosenzweig, C., & Pounds, J. A. (2003). Fingerprints of global warming on wild animals and plants. *Nature*, *421*(6918), 57–60. https://doi.org/10.1038/nature01333

Schwartz, M. D. (1992). Phenology and springtime surface-layer change. *Monthly Weather Review*, *120*(11), 2570–2578. https://doi.org/10.1175/1520-0493(1992)120<2570:PASSLC>2.0.CO;2

Schwartz, M. D., Ahas, R., & Aasa, A. (2006). Onset of spring starting earlier across the Northern Hemisphere. *Global Change Biology*, *12*(2), 343–351. https://doi.org/10.1111/j.1365-2486.2005.01097.x

Schwartz, M. D., Ault, T. R., & Betancourt, J. L. (2013). Spring onset variations and trends in the continental United States: Past and regional assessment using temperature-based indices. *International Journal of Climatology*, *33*(13), 2917–2922. https://doi.org/10.1002/joc.3625

Sitch, S., Smith, B., Prentice, I. C., Arneth, A., Bondeau, A., Cramer, W., et al. (2003). Evaluation of ecosystem dynamics, plant geography and terrestrial carbon cycling in the LPJ dynamic global vegetation model. *Global Change Biology*, *9*(2), 161–185. https://doi.org/10.1046/j.1365-2486.2003.00569.x

Song, X., Wang, D. Y., Li, F., & Zeng, X. D. (2021). Evaluating the performance of CMIP6 Earth system models in simulating global vegetation structure and distribution. *Advances in Climate Change Research*, *12*(4), 584–595. https://doi.org/10.1016/j.accre.2021.06.008

Wang, R., Gamon, J. A., Montgomery, R. A., Townsend, P. A., Zygielbaum, A. I., Bitan, K., et al. (2016). Seasonal variation in the NDVI–species richness relationship in a prairie grassland experiment (Cedar Creek). *Remote Sensing*, *8*(2), 128. https://doi.org/10.3390/rs8020128

Wang, X., Xiao, J., Li, X., Cheng, G., Ma, M., Zhu, G., et al. (2019). No trends in spring and autumn phenology during the global warming hiatus. *Nature Communications*, *10*(1), 1–10. https://doi.org/10.1038/s41467-019-10235-8

White, M. A., De Beurs, K. M., Didan, K., Inouye, D. W., Richardson, A. D., Jensen, O. P., et al. (2009). Intercomparison, interpretation, and assessment of spring phenology in North America estimated from remote sensing for 1982–2006. *Global Change Biology*, *15*(10), 2335–2359. https://doi.org/10.1111/j.1365-2486.2009.01910.x

White, M. A., Thornton, P. E., & Running, S. W. (1997). A continental phenology model for monitoring vegetation responses to interannual climatic variability. *Global Biogeochemical Cycles*, *11*(2), 217–234. https://doi.org/10.1029/97GB00330

Xu, X., Riley, W. J., Koven, C. D., Jia, G., & Zhang, X. (2020). Earlier leaf-out warms air in the north. *Nature Climate Change*, *10*(4), 370–375. https://doi.org/10.1038/s41558-020-0713-4

Zhang, X., Wang, J., Gao, F., Liu, Y., Schaaf, C., Friedl, M., et al. (2017). Exploration of scaling effects on coarse resolution land surface phenology. *Remote Sensing of Environment*, *190*, 318–330. https://doi.org/10.1016/j.rse.2017.01.001

Zhu, L., Meng, J., Li, F., & You, N. (2019). Predicting the patterns of change in spring onset and false springs in China during the twenty-first century. *International Journal of Biometeorology*, *63*(5), 591–606. https://doi.org/10.1007/s00484-017-1456-4

Zohner, C. M., Mo, L., Renner, S. S., Svenning, J. C., Vitasse, Y., Benito, B. M., et al. (2020). Late-spring frost risk between 1959 and 2017 decreased in North America but increased in Europe and Asia. *Proceedings of the National Academy of Sciences*, *117*(22), 12192–12200. https://doi.org/10.1073/pnas.1920816117

References From the Supporting Information

Bi, D., Dix, M., Marsland, S. J., O'Farrell, S., Rashid, H., Uotila, P., et al. (2013). The ACCESS coupled model: Description, control climate and evaluation. *Australian Meteorological & Oceanographic Journal*, *63*(1), 41–64. https://doi.org/10.22499/2.6301.004

Botta, A., Viovy, N., Ciais, P., Friedlingstein, P., & Monfray, P. (2000). A global prognostic scheme of leaf onset using satellite data. *Global Change Biology*, *6*(7), 709–725. https://doi.org/10.1046/j.1365-2486.2000.00362.x

Boucher, O., Servonnat, J., Albright, A. L., Aumont, O., Balkanski, Y., Bastrikov, V., et al. (2020). Presentation and evaluation of the IPSL-CM6A-LR climate model. *Journal of Advances in Modeling Earth Systems*, *12*(7), e2019MS002010. https://doi.org/10.1029/2019ms002010

Cao, J., Wang, B., Yang, Y.-M., Ma, L., Li, J., Sun, B., et al. (2018). The NUIST Earth System Model (NESM) version 3: Description and preliminary evaluation. *Geoscientific Model Development*, *11*(7), 2975–2993. https://doi.org/10.5194/gmd-11-2975-2018

Döscher, R., Acosta, M., Alessandri, A., Anthoni, P., Arneth, A., Arsouze, T., et al. (2021). The EC-Earth3 Earth system model for the climate model intercomparison project 6. *Geoscientific Model Development Discussions*, *15*, 2793–3020.

Gutjahr, O., Putrasahan, D., Lohmann, K., Jungclaus, J. H., von Storch, J.-S., Brüggemann, N., et al. (2019). Max Planck Institute Earth System Model (MPI-ESM1. 2) for the high-resolution model intercomparison project (HighResMIP). *Geoscientific Model Development*, *12*(7), 3241–3281. https://doi.org/10.5194/gmd-12-3241-2019

Hagedorn, R., Doblas-Reyes, F. J., & Palmer, T. N. (2005). The rationale behind the success of multi-model ensembles in seasonal forecasting—I. Basic concept. *Tellus A: Dynamic Meteorology and Oceanography*, *57*(3), 219–233. https://doi.org/10.3402/tellusa.v57i3.14657

Hajima, T., Watanabe, M., Yamamoto, A., Tatebe, H., Noguchi, M. A., Abe, M., et al. (2020). Development of the MIROC-ES2L Earth system model and the evaluation of biogeochemical processes and feedbacks. *Geoscientific Model Development*, *13*(5), 2197–2244. https://doi.org/10.5194/GMD-13-2197-2020

Hamdi, R., Degrauwe, D., Duerinckx, A., Cedilnik, J., Costa, V., Dalkilic, T., et al. (2014). Evaluating the performance of SURFEXv5 as a new land surface scheme for the ALADINcy36 and ALARO-0 models. *Geoscientific Model Development*, *7*(1), 23–39. https://doi.org/10.5194/gmd-7-23-2014

Haxeltine, A., & Prentice, I. C. (1996). BIOME3: An equilibrium terrestrial biosphere model based on ecophysiological constraints, resource availability, and competition among plant functional types. *Global Biogeochemical Cycles*, *10*(4), 693–709. https://doi.org/10.1029/96gb02344

He, B., Bao, Q., Wang, X., Zhou, L., Wu, X., Liu, Y., et al. (2019). CAS FGOALS-f3-L model datasets for CMIP6 historical atmospheric model intercomparison project simulation. *Advances in Atmospheric Sciences*, *36*(8), 771–778. https://doi.org/10.1007/s00376-019-9027-8

Held, I. M., Guo, H., Adcroft, A., Dunne, J. P., Horowitz, L. W., Krasting, J., et al. (2019). Structure and performance of GFDL's CM4. 0 climate model. *Journal of Advances in Modeling Earth Systems*, *11*(11), 3691–3727. https://doi.org/10.1029/2019ms001829

Ito, A., & Oikawa, T. (2002). A simulation model of the carbon cycle in land ecosystems (Sim-CYCLE): A description based on dry-matter production theory and plot-scale validation. *Ecological Modelling*, *151*(2–3), 143–176. https://doi.org/10.1016/s0304-3800(01)00473-2

Law, R. M., Ziehn, T., Matear, R. J., Lenton, A., Chamberlain, M. A., Stevens, L. E., et al. (2017). The carbon cycle in the Australian Community Climate and Earth System Simulator (ACCESS-ESM1)—Part 1: Model description and pre-industrial simulation. *Geoscientific Model Development*, *10*(7), 2567–2590. https://doi.org/10.5194/gmd-10-2567-2017

Lawrence, D. M., Fisher, R. A., Koven, C. D., Oleson, K. W., Swenson, S. C., Bonan, G., et al. (2019). The Community Land Model version 5: Description of new features, benchmarking, and impact of forcing uncertainty. *Journal of Advances in Modeling Earth Systems*, *11*(12), 4245–4287. https://doi.org/10.1029/2018ms001583

19448007, 2023, 8, Downloaded from https://agupubs.onlinelibrary.wiley.com/doi/10.1029/2023GL102833 by Cornell University, Wiley Online Library on [26/04/2023]. See the Terms and Conditions (https://onlinelibrary.wiley.com/terms-and-conditions) on Wiley Online Library for rules of use; OA articles are governed by the applicable Creative Commons License

Lee, J., Kim, J., Sun, M.-A., Kim, B.-H., Moon, H., Sung, H. M., et al. (2020). Evaluation of the Korea meteorological administration advanced community Earth-system model (K-ACE). *Asia-Pacific Journal of Atmospheric Sciences*, *56*(3), 381–395. https://doi.org/10.1007/s13143-019-00144-7

Lee, W. L., Wang, Y. C., Shiu, C. J., Tsai, I. C., Tu, C. Y., Lan, Y. Y., et al. (2020). Taiwan Earth System Model Version 1: Description and evaluation of mean state. *Geoscientific Model Development*, *13*(9), 3887–3904. https://doi.org/10.5194/GMD-13-3887-2020

Lehner, F., Deser, C., Maher, N., Marotzke, J., Fischer, E. M., Brunner, L., et al. (2020). Partitioning climate projection uncertainty with multiple large ensembles and CMIP5/6. *Earth System Dynamics*, *11*(2), 491–508. https://doi.org/10.5194/esd-11-491-2020

Lovato, T., Peano, D., Butenschön, M., Materia, S., Iovino, D., Scoccimarro, E., et al. (2022). CMIP6 simulations with the CMCC Earth system model (CMCC-ESM2). *Journal of Advances in Modeling Earth Systems*, *14*(3), e2021MS002814. https://doi.org/10.1029/2021ms002814

Mauritsen, T., Bader, J., Becker, T., Behrens, J., Bittner, M., Brokopf, R., et al. (2019). Developments in the MPI-M Earth system model version 1.2 (MPI-ESM1.2) and its response to increasing CO_2. *Journal of Advances in Modeling Earth Systems*, *11*(4), 998–1038. https://doi.org/10.1029/2018MS001400

Pak, G., Noh, Y., Lee, M.-I., Yeh, S.-W., Kim, D., Kim, S.-Y., et al. (2021). Korea institute of ocean science and technology Earth system model and its simulation characteristics. *Ocean Science Journal*, *56*(1), 18–45. https://doi.org/10.1007/s12601-021-00001-7

Rohde, R., Muller, R. A., Jacobsen, R., Muller, E., Perlmutter, S., Rosenfeld, A., et al. (2013). A new estimate of the average earth surface land temperature spanning 1753 to 2011. *Geoinformatics & Geostatistics: An Overview*, *7*, 2. https://doi.org/10.4172/2327-4581.1000101

Séférian, R., Nabat, P., Michou, M., Saint-Martin, D., Voldoire, A., Colin, J., et al. (2019). Evaluation of CNRM Earth System Model, CNRM-ESM2-1: Role of Earth system processes in present-day and future climate. *Journal of Advances in Modeling Earth Systems*, *11*(12), 4182–4227. https://doi.org/10.1029/2019ms001791

Schwartz, M. D. (1997). Spring Index Models: An approach to connecting Satellite and surface phenology. In *Phenology of seasonal climates* (Issue 414) (pp. 23–38).

Schwartz, M. D., & Marotz, G. A. (1986). An approach to examining regional atmosphere-plant interactions with phenological data. *Journal of Biogeography*, *13*(6), 551–560. https://doi.org/10.2307/2844818

Schwartz, M. D., & Reiter, B. E. (2000). Changes in North American spring. *International Journal of Climatology*, *20*(8), 929–932. https://doi.org/10.1002/1097-0088(20000630)20:8<929::aid-joc557>3.0.co;2-5

Seland, Ø., Bentsen, M., Olivié, D., Toniazzo, T., Gjermundsen, A., Graff, L. S., et al. (2020). Overview of the Norwegian Earth System Model (NorESM2) and key climate response of CMIP6 DECK, historical, and scenario simulations. *Geoscientific Model Development*, *13*(12), 6165–6200. https://doi.org/10.5194/GMD-13-6165-2020

Sellar, A. A., Jones, C. G., Mulcahy, J. P., Tang, Y., Yool, A., Wiltshire, A., et al. (2019). UKESM1: Description and evaluation of the U.K. Earth system model. *Journal of Advances in Modeling Earth Systems*, *11*(12), 4513–4558. https://doi.org/10.1029/2019MS001739

Semmler, T., Danilov, S., Gierz, P., Goessling, H. F., Hegewald, J., Hinrichs, C., et al. (2020). Simulations for CMIP6 with the AWI climate model AWI-CM-1-1. *Journal of Advances in Modeling Earth Systems*, *12*(9), e2019MS002009. https://doi.org/10.1029/2019ms002009

Swart, N. C., Cole, J. N. S., Kharin, V. V., Lazare, M., Scinocca, J. F., Gillett, N. P., et al. (2019). The Canadian Earth system model version 5 (CanESM5.0.3). *Geoscientific Model Development*, *12*(11), 4823–4873. https://doi.org/10.5194/GMD-12-4823-2019

Tatebe, H., Ogura, T., Nitta, T., Komuro, Y., Ogochi, K., Takemura, T., et al. (2019). Description and basic evaluation of simulated mean state, internal variability, and climate sensitivity in MIROC6. *Geoscientific Model Development*, *12*(7), 2727–2765. https://doi.org/10.5194/gmd-12-2727-2019

Voldoire, A., Saint-Martin, D., Sénési, S., Decharme, B., Alias, A., Chevallier, M., et al. (2019). Evaluation of CMIP6 deck experiments with CNRM-CM6-1. *Journal of Advances in Modeling Earth Systems*, *11*(7), 2177–2213. https://doi.org/10.1029/2019ms001683

Volodin, E. M., Mortikov, E. V., Kostrykin, S. V., Galin, V. Y., Lykossov, V. N., Gritsun, A. S., et al. (2017). Simulation of the present-day climate with the climate model INMCM5. *Climate Dynamics*, *49*(11–12), 3715–3734. https://doi.org/10.1007/S00382-017-3539-7

Volodin, E. M., Mortikov, E. V., Kostrykin, S. V., Galin, V. Y., Lykossov, V. N., Gritsun, A. S., et al. (2018). Simulation of the modern climate using the INM-CM48 climate model. *Russian Journal of Numerical Analysis and Mathematical Modelling*, *33*(6), 367–374. https://doi.org/10.1515/RNAM-2018-0032

Wang, Y. P., Law, R. M., & Pak, B. (2010). A global model of carbon, nitrogen and phosphorus cycles for the terrestrial biosphere. *Biogeosciences*, *7*(7), 2261–2282. https://doi.org/10.5194/bg-7-2261-2010

Wu, T., Lu, Y., Fang, Y., Xin, X., Li, L., Li, W., et al. (2019). The Beijing Climate Center Climate System Model (BCC-CSM): The main progress from CMIP5 to CMIP6. *Geoscientific Model Development*, *12*(4), 1573–1600. https://doi.org/10.5194/GMD-12-1573-2019

Yukimoto, S., Kawai, H., Koshiro, T., Oshima, N., Yoshida, K., Urakawa, S., et al. (2019). The meteorological research institute Earth system model version 2.0, MRI-ESM2.0: Description and basic evaluation of the physical component. *Journal of the Meteorological Society of Japan*, *97*(5), 931–965. https://doi.org/10.2151/JMSJ.2019-051

19448007, 2023, 8, Downloaded from https://agupubs.onlinelibrary.wiley.com/doi/10.1029/2023GL102833 by Cornell University, Wiley Online Library on [26/04/2023]. See the Terms and Conditions (https://onlinelibrary.wiley.com/terms-and-conditions) on Wiley Online Library for rules of use; OA articles are governed by the applicable Creative Commons License